Comparative Analysis of Cold In-place Recycling for Roadway Maintenance and Rehabilitation from the Perspectives of Technical-Cost-Environmental Nexus

Abstract: Cold-in-place recycling (CIR) is a sustainable road pavement maintenance technology for its on-site operation and complete reuse of reclaimed asphalt pavement. However, its sustainable performance has not been thoroughly investigated. This study aims to systematically assess and compare CIR against three alternative maintenance technologies from technical, cost and environmental perspectives, specially taking into account different numbers of repaired layers. The technical improvement in full-depth loading resistance is evaluated using a newly developed multi-sequenced repeated load (MSRL) test. Environmental impacts are assessed through life cycle assessment (LCA), while cost analysis is conducted using life cycle cost analysis (LCCA), with consistent system boundary applied. Additionally, a nexus analysis is performed using a modified Boston Consulting Group (BCG) matrix to comprehensively examine the sustainable performance of different treatments and further explore the synergies and trade-offs among various assessment aspects. The multi-dimensional sustainable assessment results reveal the influence factors in each perspective. Final BCG matrix shows that CIR can achieve the comparable technical performance to the conventional maintenance treatment, while reducing GHG emissions by 60.8% and cost by 45.8%. The methodology and findings of this study are expected to provide helpful insights for decision-makers in reducing negative impacts and promoting integrated management for sustainability.

Keywords: Cold-In-Place Recycling; Mechanical Performance; Life Cycle Assessment; Life Cycle Cost Analysis; Nexus Analysis.

1 Introduction

The roadways in China are currently facing significant demand of maintenance and rehabilitation (M&R) (Cao, Leng, & Hsu, 2019; Siverio Lima et al., 2021; Yao et al., 2019). Overlay or milling and filling (M&F) the surface layer can help restore pavement condition in most cases. However, due to increasing traffic volumes and severe overloading, road sections only undergo surface rehabilitation may still experience significant performance deterioration. Even if maintenance is performed on the upper layers, the existing asphalt mixtures in the middle layers may still lack adequate load resistance (X. Wang et al., 2018). As a result, highway agencies face the dual challenge of budgetary constraints and environmental concerns if they need to mill the old pavement down to the middle layer and completely replace it. In this context, cold in-place recycling (CIR), a sustainable rehabilitation technique, holds the potential to serve as a solution (Thenoux et al., 2007; Xiao et al., 2018; Zarrinkamar & Modarres, 2020). This technique allows for 100% reuse of reclaimed asphalt pavement (RAP) materials by using liquid asphalt binder, such as asphalt emulsion or foamed asphalt (Kim et al., 2010; Xiao et al., 2018).

From the perspective of material properties, CIR mixtures exhibit lower tensile and bending strength but good fatigue resistance when compared to the conventional hot-mix asphalt (HMA) (Gao et al., 2017; Gao et al., 2016). With specially designed binder modifications and additives, CIR mixtures can also provide rutting resistance

comparable to HMA at high temperatures (Jiang et al., 2018). Due to the high air void content in CIR mixtures, the CIR layer can hardly be used as a wearing course in pavement structures. An overlay is usually placed on top of the CIR layer to prevent early-aged moisture damage (F. Gu et al., 2019). The mechanical performance of CIR materials is quite different from those of HMA, and there is no unified specification to compare their overall performance. Therefore, it is necessary to evaluate the load resistance of the entire pavement structure after the implementation of various maintenance strategies with or without CIR techniques to understand how CIR materials affect the load resistance of the entire pavement structure. The assessment should be carried out on full-depth field cores extruded from in-service asphalt pavements. An emerging multi-sequence repeated load (MSRL) test was conducted to estimate the overall loading resistance of different pavement structures (Zhao et al., 2020). This evaluation provided valuable insights into the effectiveness of CIR in preserving the structural integrity of pavements.

In addition to the technical aspect, it is also necessary to examine and compare the cost and environmental impacts of CIR for more informed decision-making. Cost-effectiveness is the primary concern for many transportation agencies due to limited budgets. To make long-term and cost-effective decisions, these agencies have increasingly relied on life cycle cost analysis (LCCA), which is a robust economic tool that comprehensively quantifies the cost of highway construction, rehabilitation, and

maintenance (Babashamsi, Yusoff, et al., 2016; INDOT, 2005; Reigle & Zaniewski, 2002; João Santos & Ferreira, 2013). However, considering the growing attention to environmental impacts, especially climate change, decisions that solely focus on economic benefits have become outdated (Lu et al., 2023; Ma et al., 2021). Many studies have started to investigate the environmental impacts of maintenance treatments to support more sustainable decision-making in pavement management (Cao, Leng, Yu, et al., 2019; Chappat & Bilal, 2003; Chehovits & Galehouse, 2010; De Pascale et al., 2023; Giustozzi et al., 2012; J. Santos et al., 2014; Thenoux et al., 2007; T. Wang et al., 2018). Among these studies, life cycle assessment (LCA) has been a popular method for evaluating the environmental impacts of different pavement M&R techniques. Although several researchers (Chiu et al., 2008; Giani et al., 2015; Turk et al., 2016) have conducted comparative LCA studies on CIR and traditional mill-and-overlay techniques, the impact of different treated layers and their thicknesses has not been considered in the previous LCA scenarios, considering the typical pavement structure consists of base layer, middle layer, and upper layer, each with varying thickness.

Despite the quantification of technical, cost, and environmental performance, it is still necessary to explore the interaction among different sustainable aspects. Nexus analysis allows for the simultaneous examination of the interconnections, uncovering synergies, and detecting trade-offs among multiple dimensions (Liu et al., 2018). Portfolio analysis, as one of the nexus approaches, can combine multidimensional indicators into

a categorized portfolio for more strategic decision-making. Several methods have been developed for portfolio analysis (Grünig & Kühn, 2018), with the widely applied tool being the Boston Consulting Group (BCG) matrix. It was initially developed for optimizing business strategy based on product market share and market growth (Barksdale & Harris, 1982). The rule-based BCG matrix can integrate two-dimensional variables and comprehensively analyze performance from two perspectives. Subsequently, the matrix portfolio parameters have been modified and applied to various areas beyond product business strategy (Ha et al., 2021; Khairat & Alromeedy, 2016; Shen et al., 2021; Singh, 2004). This study initially integrates the bi-dimensional BCG matrix with bubble chart to visualize the numerical relationships among the three-dimensional variables. It extends the application of BCG matrix in the sustainability and construction fields for environment-cost-performance nexus analysis.

In this study, a comprehensive analysis framework was established. The load resistance performance, global warming potentials (GWP), and cost of CIR and other three maintenance alternatives were evaluated, followed by a three-dimensional integration using the modified BGC matrix. The analysis was conducted based on a real case study, specifically considering the influences of the number of treated layers and different prior pavement conditions.

2 Methodology

The analysis in this study was carried out in four steps: 1) technical performance evaluation, 2) environmental performance evaluation, 3) economic performance evaluation, and 4) nexus analysis. A three-dimensional evaluation framework (technique, environment, and economic) was developed, and the impact factors in each dimension were identified. The performance was then visualized in the modified BCG matrix for nexus analysis, which aimed to uncover synergies and detect trade-offs among different evaluation dimensions. Figure 1 illustrates the methodological framework, as well as the methods, indicators, and goals of the assessment in the various dimensions.

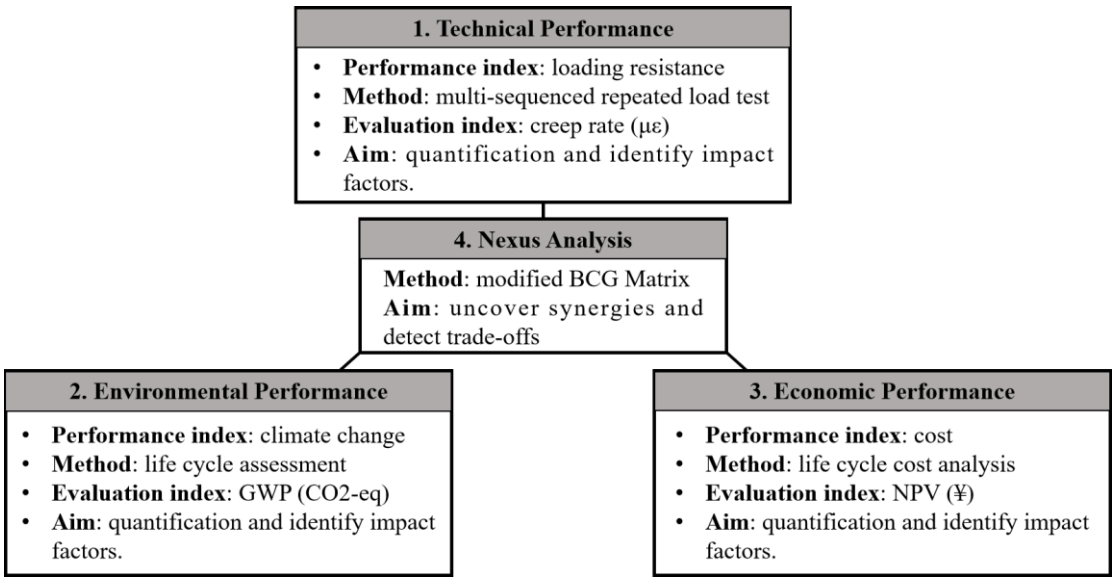

Figure 1. Methodological framework in this study

2.1 Technical performance

The multi-sequenced repeated load (MSRL) test was conducted on full-depth field

cores to examine the load resistance of pavement structures under laboratory test conditions. These conditions closely resembled the actual field conditions in terms of temperature, axle-load spectrum and boundary. Previous research has extensively discussed the procedure of this newly developed MSRL test and its applicability to full-depth field cores (Jiang et al., 2016). This test consists of two steps: multi-sequenced loading and simulations of temperatures and boundaries.

2.1.1 Multi-sequenced loading

The permanent deformation of asphalt mixtures, measured in terms of loading times, exhibits a three-stage behavior and shows a nearly constant creep rate in the second stage (Zhou & Scullion, 2002). Higher creep rates in the second stage indicate poorer load resistance of asphalt materials and a faster accumulation of distress. To ensure that the full-depth samples reached the creep stage, a pre-loading sequence with a stress level of 700Kpa and 1000 loading times was applied. Considering the complexity of actual axle loads, six stress levels ranging from 600KPa to 1100KPa were applied to the full-depth field cores, and each stress level was loaded for 100 times, as shown in Figure . The multi-sequenced repeated load was then repeated five times continuously to obtain the most stable creep rate at each stress level. A power function, as shown in Equation 1, was used to fit the relationship between creep rates and stress levels. Each load cycle lasts one second, consisting of a 0.1 second half-sine wave load and a 0.9 second rest period. The average axle load spectrum of the target road section over the

past five years was obtained from the pavement management system (PMS) in Jiangsu province of China.

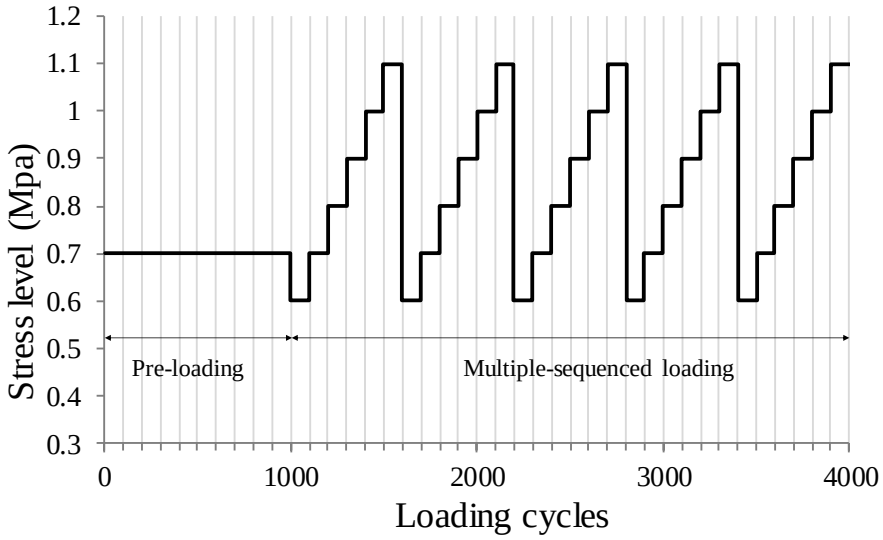

Figure 2. Loading configuration for the MSRL test

Figure 3 illustrates the axle load spectrum of a road section on the highway route S49, along with its typical parameters. The weigh-in-motion (WIM) system was used to measure the repeated occurrences of 13 different axle load internals. The representative axle load for each interval was determined by taking the mid-value of the interval and converting it to a stress level using Equation 2 (Jiang et al, 2016). The rutting index, known as the compound creep rate (CCR), was then calculated from the MSRL test by Equation 3. This index represents the weighted mean of the corresponding creep rate calculated by Equation 1 for the 13 different axle load intervals.

$$\varepsilon(\sigma)=a\cdot\sigma^{b} \quad (1)$$

$$\frac{\sigma_i}{\sigma_s}=\left(\frac{q_i}{q_s}\right)^{0.65} \quad (2)$$

$$\varepsilon_c = \sum_{i=1}^{13} \varepsilon(\sigma_i) \cdot p_i \quad (3)$$

where σ = stress level (Kpa), ε(σ) = the corresponding creep rate under the stress level σ (με), a, b = regression coefficients, ε_c = CCR based on axle load spectrum (με), i = number of the axle load interval, σ_i = the representative stress level under axle load range i (Kpa), q_i = the representative axle load of interval i (KN), σ_s = the standard tire pressure (700Kpa), q_s = the standard axle load (100KN), $\varepsilon(\sigma_i)$ = the corresponding creep rate under stress level σ_i (με), and p_i = percentage of repeated times of axle load interval i.

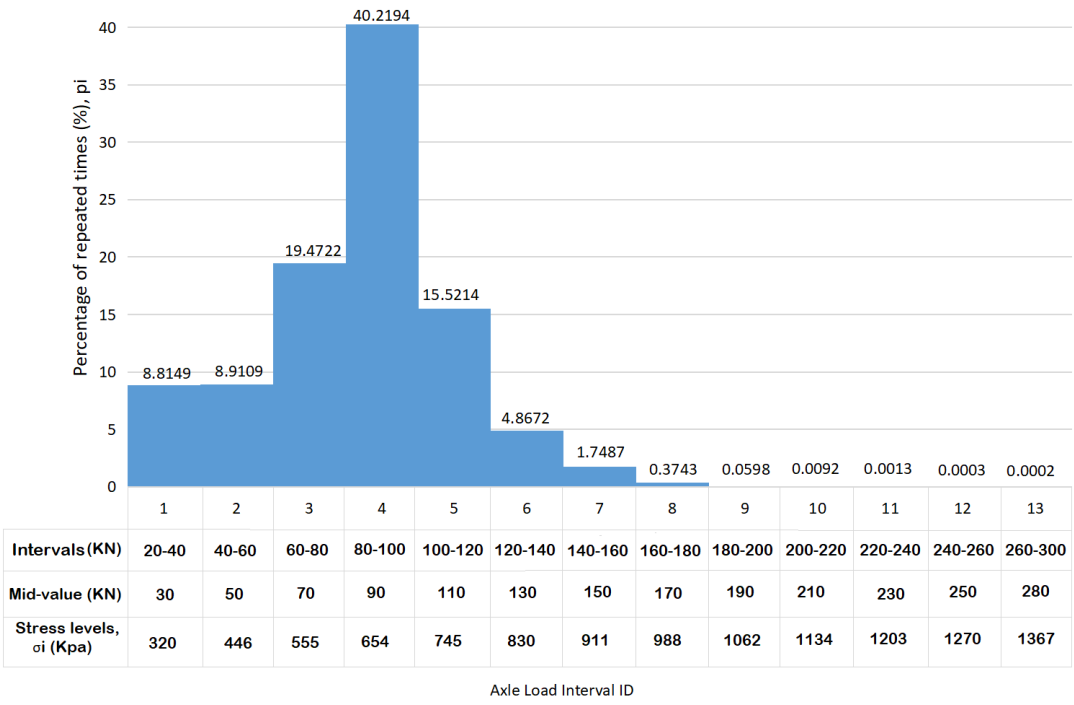

	1	2	3	4	5	6	7	8	9	10	11	12	13
Intervals (KN)	20-40	40-60	60-80	80-100	100-120	120-140	140-160	160-180	180-200	200-220	220-240	240-260	260-300
Mid-value (KN)	30	50	70	90	110	130	150	170	190	210	230	250	280
Stress levels, σi (Kpa)	320	446	555	654	745	830	911	988	1062	1134	1203	1270	1367

Figure 3. The axle load spectrum and parameters of a road section on the S49

2.1.2 Simulation of temperature and boundary

To replicate the temperature gradient of the pavement surface in the field, special treatment was applied to the full-depth field cores, as depicted in Figure 4(a). The outer

surface of the samples was coated with heat insulation materials to ensure that only the top surface could exchange heat with the outside air, while the bottom and sides of the samples were insulated (X. Gu et al., 2014). The chamber temperature was set at 62℃, which represents the extreme temperature of the pavement surface on the selected expressway. To achieve a better boundary condition, a small plate with a 5cm diameter was used as the pressure head for the vertical loading, as illustrated in Figure 4(b). A UTM-25 loading machine was utilized for the MSRL test. The test continued until either the accumulated micro-strain reached 50,000 or the loading cycles reached 4,000. Two replicated field cores were prepared for the MRSL test for each pavement structure, either before or after maintenance.

(a) (b)

Figure 4. Set-up of the MSRL test: (a) Surface treatment; (b) Loading equipment.

2.2 Environmental performance

Life Cycle Assessment (LCA) was implemented to evaluate the environmental impacts

following the international standards ISO 14040 (ISO, 2006). The assessment involved four major steps: 1) goal and scope definition, 2) life cycle inventory (LCI) analysis, 3) life cycle impact assessment, and 4) interpretation.

2.2.1 Goal and scope definition

The goal of this LCA study is to provide scientific knowledge regarding the environmental benefits of CIR and make recommendations for prioritizing future pavement maintenance. The study quantifies and analyzes the global warming potential (GWP) of CIR, comparing it with other alternative maintenance treatments. The functional unit used is 1 km-lane within the "cradle-to-site" system boundary. Figure 5 illustrates the four-stage LCA system for asphalt pavement maintenance treatments: (1) material production stage, (2) construction stage, (3) transportation stage, and (4) end-of-life (EOL) stage.

The material production stage quantifies the environmental impacts associated with producing the materials required for the maintenance treatment, such as asphalt binders, aggregates, cement, and hot asphalt mixtures. Asphalt binders are extracted from crude oil at refinery, and can be modified by adding polymer or emulsion for the different performance enhancements. Aggregates are mined from nature hard rock, and crushed to course, fine, filler sizes. Then, the aggregates and asphalt binders are mixed at high temperature to obtained the desired surface textures for asphalt mixtures based on

required ratios and gradations, such as stone mastic asphalt (SMA), dense-graded asphalt concrete (AC), and Surperpave (SUP). The construction stage evaluates energy loads from maintenance activities, including milling, sweeping, paving, cold-in-place recycling, and compaction. The transportation stage calculates the environmental impacts of material transportation processes, such as transporting asphalt binder from the refinery site to the mixing plant, aggregates from local quarry to the mixing plant, hot asphalt mixture from the mixing plant to the construction site, and milled old pavements for disposal. In the EOL stage, no environmental burdens are assigned due to the "cut-off" allocation rule, assuming that the EOL pavement surface will be completely reclaimed on-site and serve for the next life cycle system.

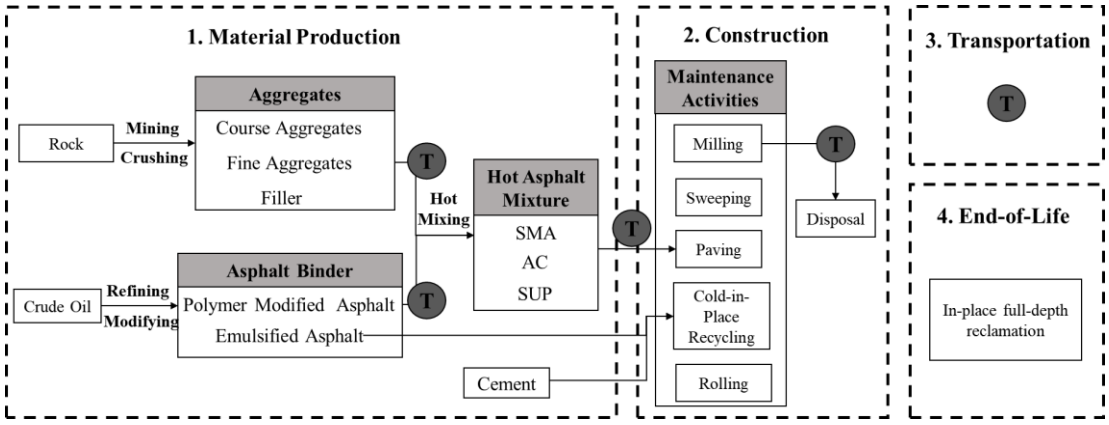

Figure 5. Life cycle system model of asphalt pavement maintenance treatments

2.2.2 Life cycle inventory analysis

LCI quantifies the environmental inputs and outputs of unit processes within the defined life cycle stages outlined in the goal and scope definition (ISO, 2006). Inventory

data forms the foundation of LCA and typically contains foreground and background data. Foreground data refers to the information used to model the unit process of each life stage for establishing goal system, which may vary in different practical application scenarios. Background data are collected from various data sources and provide the environmental input and output of each unit process to the foreground system for quantification and analysis (US EPA, 2006).

2.2.3 Life cycle impact assessment

The life cycle impact assessment aims to characterize the extensive list of life cycle inventory results into a limited number of environmental impact categories (ISO, 2006). In this study, the GWP was chosen as representative indicator to reflect the environmental performance. GWP integrates the calculated radiative forcing contribution from an idealized pulse emission over a selected time horizon (IPCC, 2021), and it has been widely regulated by policies and laws (UNFCCC, 1998, 2015). It is worth to mention that the total GWP-weighted emissions of a set of emissions may not be equal to the temporal evolution of climate response. Given the "cradle-to-site" scope of this study and the relatively short time span considered, GWP values for 100-year time horizon were applied. This time horizon has been widely adapted since the Kyoto Protocol (UNFCCC, 1998). It aggregates the greenhouse gas (GHG) emissions in CO_2-eq, such as carbon dioxide (CO_2), methane (CH_4), and nitrous oxide (N_2O) (IPCC, 2021).

2.3 Economic performance

To quantify the economic performances of different maintenance alternatives, Life Cycle Cost Analysis (LCCA) was conducted based on the concept of net present value (NPV), which includes all costs incurred during the production, use and disposal (Babashamsi, Md Yusoff, et al., 2016). In order to maintain consistency in the analysis scope with LCA, this study takes into account the costs generated by different maintenance treatments throughout the defined life cycle stages , including material production stage, transportation stage and construction stage.

2.4 Nexus analysis

Once the performance in different dimensions has been evaluated, nexus analysis was conducted by calculating and plotting the nexus performance portfolio onto the modified BCG matrix. As shown in Figure 6, each bubble in the plot represents a maintenance alternative, with cost performance on the horizontal axis and environmental impact on the vertical axis. The size of the bubble reflects the level of technical performance improvement achieved by the corresponding treatment.

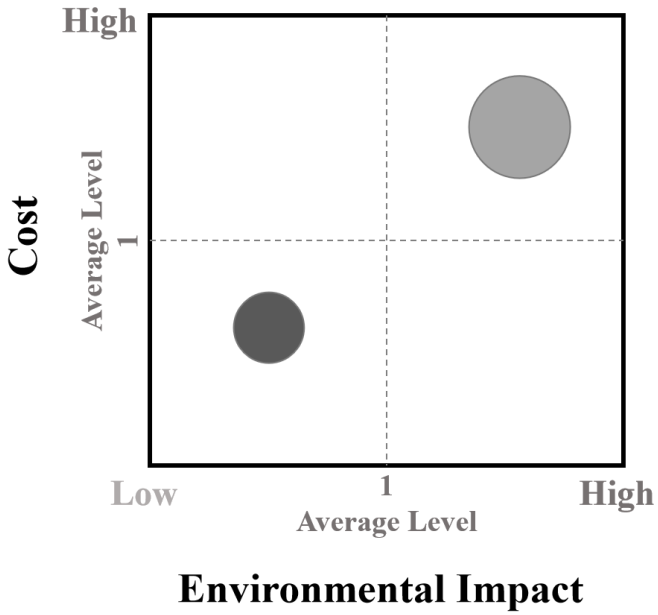

Figure 6. Schematic of the BCG matrix for nexus analysis

The location of the portfolio is determined by the relative environmental and cost performance, calculated using Equation 4 and 5. The median lines on horizontal and vertical axises represent the average performance levels of the alternatives. A lower value in environmental impact and cost (lower left corner) indicates better performance. Therefore, alternatives that perform superior in terms of cost, environment and technique will be positioned closer to the left and down side with a larger bubble size.

$$P_{E,\alpha} = \frac{EI_\alpha}{(\sum EI)/_j} \quad (4)$$

$$P_{C,\alpha} = \frac{NPV_\alpha}{(\sum NPV)/_j} \quad (5)$$

where $P_{E,\alpha}$= environmental impact portfolio position for alternative α, $P_{C,\alpha}$= cost performance portfolio position for alternative α, EI_α = environmental impact for alternative α, NPV_α = net present value for alternative α, and j = number of alternatives under considerations.

3 Case Study

3.1 Foreground information

In this study, the evaluation framework presented in the previous section was implemented in a case study of highway maintenance project on the Xinyang highway S49 in the north region of Jiangsu Province, China. The S49 is a two-way four-lane highway with a total length of approximately 137km, which has been opened to traffic since December 2000. Due to the increasing service time and traffic volume, a resurfacing and pavement maintenance project was initiated on S49 in 2018. To investigate and compare the maintenance improvement of the CIR treatment with other conventional M&R treatments, considering the effect of layer number and prior conditions, four distinct M&R treatments were selected from the four sections on S49 (S49-1, S49-2, S49-3 and S49-4) with different pre-treatment conditions. Table 1 presents the four maintenance treatments and their corresponding execution sections, labeled as A, B, C, and D. Treatment A involves a direct overlay on the old surface, treatment B includes M&F the upper layer followed by an overlay, treatment C involves M&F both the upper and middle layers followed by an overlay, and treatment D consists of CIR both the upper and middle layers followed by an overlay. The detailed processes of each treatment are outlined in Table 1. The different maintenance choices were primarily determined by the rutting depth (RD_b) of pavement before maintenance work. Treatment A and B were implemented on section S49-1 and S49-3, respectively, which had pre-treatment RD_b of less than 10mm and between 10 and 15mm, respectively. In section S49-2, both treatment A and B were utilized. For section S49-4, both treatments

C and D were applied since the pre-treatment RD_b exceeded 15mm.

Table 1. Summary of the maintenance treatment A, B, C, and D.

Treatment	RD_b (mm)	Schematic	Description	Route
A	<10	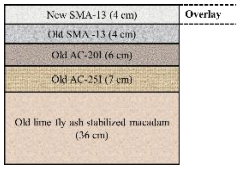	• Overlay 4cm modified SMA-13 asphalt mixtures	S49-1 S49-2
B	10-15	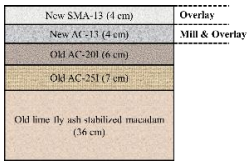	• Mill the old top layer • Fill with modified AC-13 asphalt mixtures • Overlay 4cm modified SMA-13 asphalt mixtures	S49-2 S49-3
C	>15	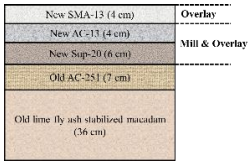	• Mill the old top and middle layers • Fill the top and middle layers with modified AC-13 and SUP-20 asphalt mixtures, respectively • Overlay 4cm modified SMA-13 asphalt mixtures	S49-4
D	>15	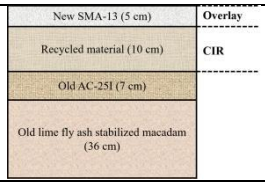	• CIR both the old top and middle layers • Overlay 5cm SMA-13 modified asphalt mixtures	S49-4

The HMA and CIR materials and their mix designs utilized in the maintenance work are specified in Table 2. For all overlay options in different treatment alternatives, stone mastic asphalt mixtures (SMA-13) with an SBS modified binder were used, adhering to the Superpave grading of PG76-22. In the case of CIR, the mixtures consist of 100% RAP from both the old top and middle layers, employing a modified asphalt emulsion and an appropriate amount of water and cement.

Table 2 Material information of the asphalt mixtures.

	Passing percentage (%)			
Sieving size (mm)	SMA-13	AC-13	SUP-20	CIR-20
26.5	100	100	100	100
19	100	100	86.1	99.7
16	100	100	70.3	96.1
13.2	92.3	93.4	58.9	89.3
9.5	59.9	65.8	41.9	74.4
4.75	25.2	37.4	31.5	44.8
2.36	20.0	30.5	25	23.5
1.18	17.7	23.8	19.1	11.5
0.6	15.2	16.8	15	6.7
0.3	13.4	11.9	12.1	2.5
0.15	11.9	8.7	9.1	1.3
0.075	10.0	6.0	7.8	0.5
Binder type	SBS modified asphalt	SBS modified asphalt	SBS modified asphalt	Emulsified asphalt
Optimal asphalt content (%)	5.90	5.10	4.50	3.30

Based on the construction processes outlined in Table 1, Table 3 identified the specific activities of construction equipment, including quantity, engine power, productivity and working hours required to construct a functional unit of pavement. The equipment used in the construction activities has typical horsepower, which is the same for all treatments in this study. For the traditional M&F, there are primarily three steps: cold milling, paving with new asphalt mixtures, and compaction. These steps are performed using a series of construction equipment, including milling machine, sweeping machine, paver, and roller, etc. In the case of CIR, the set of equipment includes a CIR machine and tank truck. The reclaimed asphalt mixtures were directly recycled in the milling

step by adding 3.3% emulsified asphalt and 2.2% cement. In this study, the milling machine is 2 meters wide and requires two passes to complete the milling task for one lane. The paver is capable of paving a single lane with a thickness of 4 to 5 cm with 1 lift. The compaction of different layers vary in speed due to the different mixture designs. The SMA-13 layer requires initial compaction at 3 km/h and recompaction at 4.5 km/h. For AC-13 layer, the compaction work can be completed using a 2-meter steel-wheel roller (10t) with initial compaction at 2 km/h, recompaction at 3.5 km/h, and final compaction at 3.5 km/h. The SUP-20 layer only requires initial compaction at 3 km/h and recompaction at 3 km/h. For the CIR layer, all compactions were performed at 3 km/h. The number of initial compaction, recompaction, and final compaction is 2, 4, and 2, respectively.

Table 3. Construction information for the maintenance treatments: A, B, C, and D

<table>
<tr><td colspan="2" rowspan="2">Equipment</td><td rowspan="2">Milling Machine</td><td rowspan="2">Sweeping Machine</td><td rowspan="2">Paver</td><td colspan="2" rowspan="2">Steel-Wheel Roller</td><td colspan="2">CIR Set</td></tr>
<tr><td>CIR Machine</td><td>Tank Truck</td></tr>
<tr><td colspan="2">Engine Power (hp)</td><td>750</td><td>100</td><td>300</td><td colspan="2">300</td><td>950</td><td>133</td></tr>
<tr><td colspan="2" rowspan="3">Productivity</td><td rowspan="3">0.5 m/min</td><td rowspan="3">0.5 m/min</td><td rowspan="3">2.5 m/min</td><td>Initial compaction</td><td>2-3 km/h</td><td colspan="2" rowspan="3">7m/min</td></tr>
<tr><td>Recompaction</td><td>3.5-4.5 km/h</td></tr>
<tr><td>Final compaction</td><td>3-3.5 km/h</td></tr>
<tr><td colspan="2">Quantity</td><td>3</td><td>2</td><td>1</td><td colspan="2">2</td><td colspan="2">1</td></tr>
<tr><td rowspan="3">Working hours (h)</td><td>A</td><td>0</td><td>0</td><td>6.67</td><td>SMA-13</td><td>3.11</td><td>0</td><td></td></tr>
<tr><td>B</td><td>66.67</td><td>66.67</td><td>12.23</td><td>AC-13
SMA-13</td><td>5.43
3.11</td><td colspan="2">0</td></tr>
<tr><td>C</td><td>66.67</td><td>66.67</td><td>17.79</td><td>SUP-20</td><td>4.00</td><td>0</td><td></td></tr>
</table>

				AC-13	5.43	
				SMA-13	3.11	
D	0	0	6.67	CIR mix	5.33	2.38
				SMA-13	3.11	

The transportation was carried out using 15-ton heavy-duty diesel trucks. These trucks were responsible for hauling raw materials, such as asphalt binders and aggregates, to the mixing plant (100 km), hauling hot asphalt mixtures to construction site (100 km), and hauling milled pavements for disposal (50km). It was assumed that the travel would include a 100% full fronthaul and an empty backhaul.

3.2 Full-depth MSRL test

To analyze and compare the high-temperature performance comprehensively, MSRL test was conducted on the full-depth field cores of pavement structures before and after maintenance. The used sampling method is demonstrated in Figure 7. For the old pavement, field cores were obtained from four road sections: S49-1, S49-2, S49-3, and S49-4. Following the completion of maintenance works, field cores of the newly maintained pavement were collected from these four road sections, including treatment A at S49-1 and S49-2, treatment B at S49-3 and S49-2, treatment C at S49-4, and treatment D at S49-4. Each sampling section had a length ranging from 200 to 500 meters. To ensure representativeness, three different coring points were selected on each section with a minimum distance of 50m between them, labeled as station 1, 2 , and 3 in Figure . Two field cores were collected at each coring point on the old pavement,

while only one field core was extruded at each coring point on the newly maintained pavement. Therefore, six replicated samples were prepared for the old pavement structure and three replicated samples were prepared for the newly maintained pavement structure for each road section.

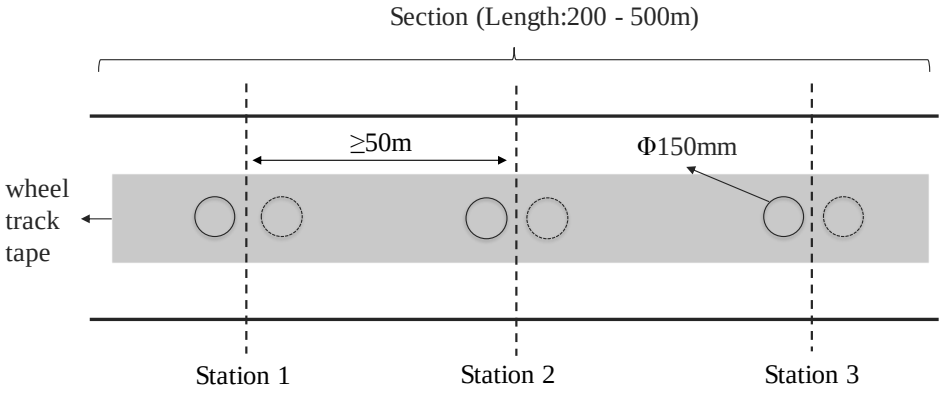

Figure 7. Scattergram of sampling methods in the field.

3.3 Life cycle assessment

Based on the LCA system modeled using foreground data, the background data were collected from various data sources during the life cycle inventory analysis to determine the energy consumption of each defined unit process. Table 4 provides a synthesis of the energy input for the processes in each life cycle stage. In the material production stage, data on the secondary energy consumption were collected. For this study, the impact of aggregate particle size on fuel consumption was excluded. The energy required for transportation was calculated by fuel consumption throughout the on-road vehicle operations. The energy consumption during construction stage was attributed to the fuel used to power non-road construction equipment. Fuel rates were measured

based on the equipment horsepower, using brake specific fuel consumption (BSFC) determined through the nonroad compression ignition (CI) engine model in MOVES3.0.2 (EPA, 2021). The data used correspond to the Tier 4 standard, which represent current and future technology for most CI engines (EPA, 2021).

Table 4. Energy input of the life cycle model of the pavement intervention

Life cycle stage	Process	Sub-process	Energy input*	Data source
Material production (MJ/t)	Asphalt	Crude oil extraction	Diesel: 522.46	Eurobitume (2011)
		Transport	Diesel: 19.29	
		Asphalt refinery	Diesel: 103.42 Nature gas: 291.06 Electricity: 8.7	
		Asphalt storage	Nature gas: 52.45 Diesel: 18.6 Electricity: 9.7	
	SBS modified Asphalt	SBS	Natural gas: 1060.58 Diesel: 420.06 Coal: 142.26	
		SBS modified Asphalt	Electricity: 72	
	Emulsified Asphalt	Emulsifier	Natural gas: 3.91; Diesel: 28.42 Coal: 0.52 Electricity: 9.65	
		Hydrochloric acid	Natural gas: 4.63 Diesel: 6.90 Coal: 2.63 Electricity: 19.30	
		Water heating	Natural gas: 59.6 Diesel: 14.3	
		Emulsified asphalt	Electricity: 111	
	Crushed Aggregate	Transport	Diesel: 17.44	Stripple (2001)
		Crushed aggregate	Diesel: 16.99 Electricity: 21.19	
	Cement		Electricity: 390	
	HMA		Diesel: 285	

		Electricity: 36	
Transportation (MJ/km)	Full-load	Diesel: 14.06	
	Empty-Load	Diesel: 10.45	
Construction (MJ/op. hr**)	Milling machine	Diesel: 4994.14	(EPA, 2021)
	Sweeping Machine	Diesel: 740.28	
	Paver	Diesel: 1997.65	
	Steel-Wheel Roller	Diesel: 1997.65	
	CIR set	Diesel: 7211.53	

Notes: *The net calorific values for diesel is 42.65 MJ/kg, for natural gas is 35.59 MJ/kg, for coal is 26.34 MJ/kg, and for electricity is 3.6 MJ/kWh.

**op.hr refers to operation hour.

All of these data represent primary energy consumption related to materials or process, which allows for traceability when quantifying their energy consumption impacts based on different regional contexts, such as different energy structures in different regions. To adapt the measures to local conditions, this study incorporated the factors based on the current situation in China, which are itemized below. 1). The average net calorific values of different energy types, as obtained from the China Energy Statistical Yearbook (National Burea of Statistics, 2020) were employed in the calculation process to maintain the consistency of energy consumption units (MJ); 2). The energy consumption for the crude oil extraction data in Middle East were employed (Eurobitume, 2011). Considering that China has become the world's largest net importer of crude oil, with the Middle East remaining the largest source of China's crude oil imports (Masnadi et al., 2018); 3). Procedures powered by electricity sourced from coal-fired power plants were considered, as coal accounted for 64.7% of electricity generation in China in 2019 (National Burea of Statistics, 2020). By considering these factors, this LCA study aimed to accurately reflect the energy

consumption associated with the processes analyzed in the context of China's energy landscape.

The GHG emissions were assessed based on fuel types and consumption patterns accordingly. The GHG gas considered in this study are CO_2, CH_4, and N_2O. Both upstream fuel production and downstream fuel use emissions were taken into account. For fuel production emissions, local emission factors from the China Products Carbon Footprint Factors Database (Chinese Academy of Environmental Planning et al., 2022) were used for calculations. These factors provide specific information on the emissions associated with fuel production processes. Regarding converting the fuel use in each stage into emissions, the emission factors from the IPCC emission factor database (EFDB) were employed. This guideline assists countries and regions in fulfilling their reporting commitments under the United Nations Framework Convention on Climate Change (UNFCCC) by providing a standardized method for quantifying anthropogenic emissions from various sources (IPCC, 2006). For the material production stage, GHG emissions were quantified based on emission factors for stationary combustion in the manufacturing industry. These factors capture the emissions associated with the combustion of fuels used in manufacturing processes. Transport emissions were assessed using emission factors specific to diesel-drive heavy-duty trucks with a gross vehicle weight less than 16 tons, driving under urban conditions. In the construction stage, GHG emissions were evaluated based on the emission factors for off-road mobile

sources and machinery.

The environmental impact was subsequently characterized using the GWP over a 100-year time horizon (GWP-100) to offer an overall measure of environmental performance for further analysis. The GWP-100 values employed in this study were obtained from the IPCC Sixth Assessment Report (AR6). These values have been refined compared to the previous fifth version, taking into account factors such as radiative properties, atmospheric lifetimes, and indirect contributions of the different gases (IPCC, 2023).

3.4 Life Cycle Cost Analysis

The LCCA analysis for this study considered the agency costs, which includes all the direct costs incurred in carrying out construction and installation works of the four compared treatments. According to the current regulations of China (Ministry of Housing and Urban-Rural Development & Ministry of Finance, 2013), the direct construction costs include labor cost, material cost, construction machinery cost, and measure fee. In order to ensure consistent cost evaluations across different treatment projects for comparative purposes, this study excluded the additional construction expenses, such as measure fee (e.g., additional expenses for winter construction), regulate fee, administrative expenses, profit, and tax. Table 5 lists the fee rates for the items included in the cost evaluation for the related maintenance activities in this study,

which were calculated via dividing the direct costs by the quantity of work based on the prices in 2019. In this study, the prices used for calculations were the net present values in 2019. The inflation rate was not considered in this study because the cost analysis only included labor, material, and construction expenses, and the construction timeline was less than a year. Additionally, it's important to note that the main objective of this study was to compare the costs of different maintenance treatments. Therefore, whether or not the same inflation rate was applied to all treatments did not have an impact on the comparative results.

Table 5. Fee rates for corresponding project items

Item	Unit	Labor cost	Material cost	Construction machinery cost
Milling	CNY/m^3	63.60	68.00	74.72
SMA-13	CNY/m^3	5.01	1782.30	631.15
AC-13	CNY/m^3	4.61	1620.03	616.84
SUP-20	CNY/m^3	4.61	1478.85	620.12
CIR	CNY/m^2	0.35	101.97	5.24

4 Results and Discussion

The technical, environmental, and economic performance of the four pavement M&R treatments were extensively evaluated in this study. The sustainable performance was assessed by rutting resistance, GWP, and cost. These assessments were conducted through various methods, such as MSRL test, LCA, and LCCA. The factors influencing each dimension were identified accordingly. The nexus analysis further integrated the multi-dimensional performance of the four M&R treatment alternatives, examining the

interactions among the performance indicators in multiple dimensions.

4.1 Loading resistance of the full-depth pavement samples

To accurately characterize the prior rutting resistance of the pavement structures, the full-depth field cores were tested by the MSRL test. Figure displays the creep curves obtained from the full-depth MSRL test for various samples. The power function fitting results and the calculated CCR of each field samples are presented in Table 6. The R^2 value of each sample exceeds 0.95, indicating an excellent fit between the creep rate and the compressive stress level.

Table 6 Testing results of the rutting resistance for the road sections before and after treatments.

Road section	Treatment	Fitting parameters			Compound creep rate	
		a	b	R^2	Mean (με)	COV
S49-1	Prior	3.0E-08	2.721	0.991	1.233	13%
	A	3.0E-09	3.094	0.991	1.472	17%
S49-2	Prior	3.0E-08	2.969	0.983	6.508	21%
	A	3.0E-07	2.534	0.984	3.823	15%
	B	3.0E-08	2.788	0.996	1.999	13%
S49-3	Prior	5.0E-09	3.085	0.986	2.458	16%
	B	3.0E-10	3.311	0.990	0.609	15%
S49-4	Prior	1.0E-08	3.150	0.985	7.331	14%
	C	4.0E-09	2.872	0.987	0.526	18%
	D	2.0E-07	2.399	0.994	0.570	14%

As depicted in Figure (a), significant differences can be observed in the creep curves of full-depth field cores obtained from the four road sections of S49. The accumulative

creep strains of full-depth samples from S49-2 and S49-4 are similar and notably higher compared to S49-1 and S49-3. According to the data in Table 6, the CCR of the full-depth samples from S49-4 is more than six times that from S49-1. This suggests that the loading resistance of full-depth samples from S49-4 is expected to be the poorest among the four road sections due to its deeper pre-treatment rutting depth (more than 15mm). However, for road section S49-2, although the rutting depth is similar to that of S49-1 and S49-3, the CCR for S49-2 is significantly higher, which may be attributed to the differences in maintenance history.

Figure 8(b) demonstrates the creep curves of various full-depth samples from different road sections after different maintenance treatments. Combined with the data in Table 6, it can be observed that road section S49-4, maintained by treatment C, presents the best high-temperature stability. This aligns with expectations since more of the old materials were replaced during treatment C. For treatment D, which involves the CIR technique, the CCR of the full-depth samples is 0.57. Although slightly higher than treatment C, it is significantly lower than treatment A and B. This indicates that the CIR technique displays remarkable performance recovery in terms of rutting resistance for the full-depth pavement structures. Besides, it is evident that applying the same treatment to different road sections can lead to significantly different rutting properties after maintenance. This is due to variations in pre-treatment performance of old pavement structures. For instance, after treatment A, the CCR of full-depth samples

from S49-2, is approximately 2.5 times higher than that of samples from S49-1. Similarly, after treatment B, the CCR of full-depth samples from S49-2 is nearly 3 times higher than that of samples from S49-3. These findings highlight the significant influence of the pre-treatment pavement condition on the effectiveness of maintenance treatments. It suggests that the initial state of the pavement structure plays a crucial role in determining the outcomes of the maintenance interventions. It affects the effectiveness of repairs and the selection of appropriate interventions. Therefore, it is important to consider the initial condition of the pavement when planning and implementing maintenance activities to ensure optimal outcomes.

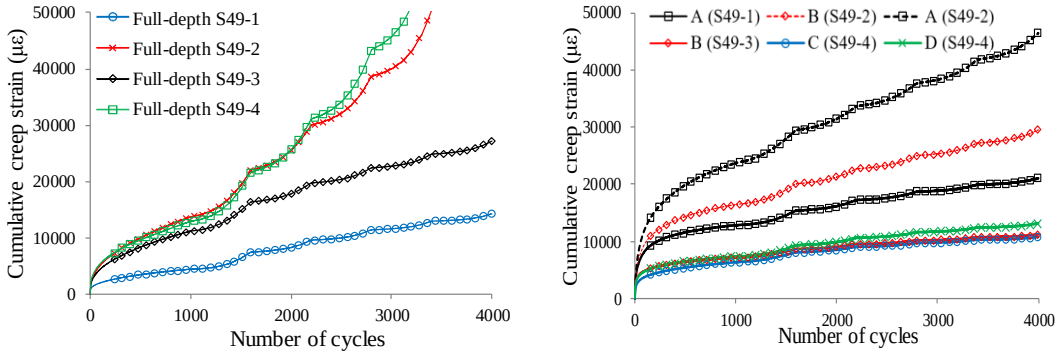

(a) (b)

Figure 8. The creep curves of the samples from different sections under the full-depth MSRL test: (a) prior performance; (b) performance after treatment

4.2 Environmental performance

The LCA was conducted for treatments A, B, C, and D using equivalent functional units, system boundaries, allocation methods and energy evaluation methods. Figure 9

illustrates the accumulated life-cycle results of GWP for the four treatments. It is evident that, in the cases of traditional M&R treatments, the GWP value increases with the number of layers treated. Treatment A (single overlay) has the least GWP value (2.37E+04 CO_2eq kg/km-lane), while treatment B (milling upper layer and overlay) contributes 5.61E+04 CO_2eq kg/km-lane GWP. Treatment D (milling upper and middle layers and overlay) is identified as having the highest GWP value (8.97E+04 CO_2eq kg/km-lane). However, CIR technique (treatment D) achieves the refurbishment of both upper and middle layers with a lower GWP contribution of 3.52E+04 CO_2eq kg/km-lane, which can reduce 60.81% GWP compared with treatment C, and falls between the GWP values of treatment A and B.

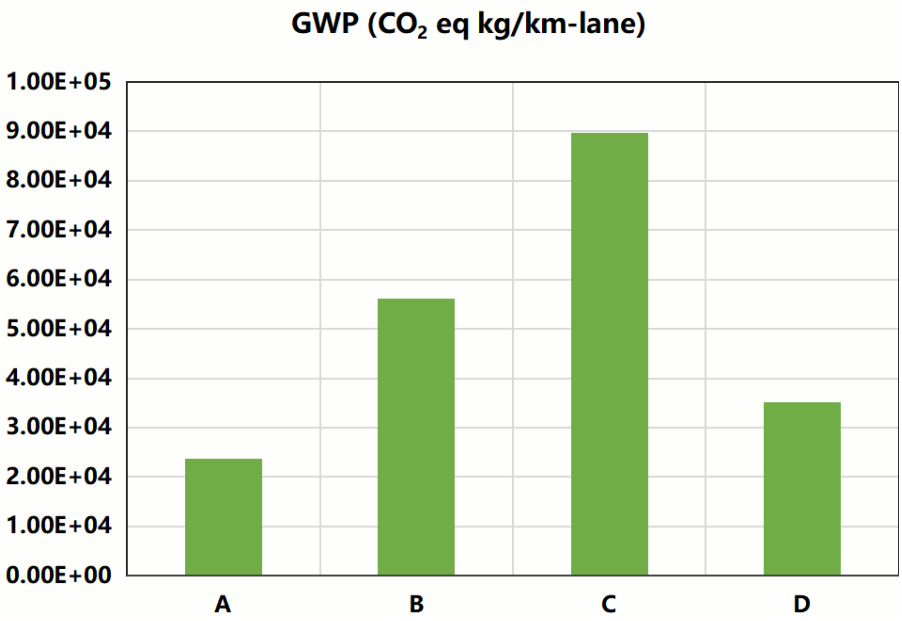

Figure 9. GWP of pavement maintenance treatment A, B, C, and D

Figure 10 provides the breakdowns of the life-cycle GWP results, including the life

cycle stages and energy consumption associated with the four compared M&R treatment alternatives.

According to Figure 10(a), the breakdown of GWP contributions based on life cycle stages reveals a common feature among all treatment alternatives. The material production stage accounts for the largest proportion of GWP, specifically 89.4% for treatment A, 74.1% for treatment B, 79.3% for treatment C, and 89.8% for treatment D. This highlights the significant impact of material production on the overall environmental footprint of the pavement life cycle, from cradle to site. The contributions from the transportation stage are relatively consistent across all treatment alternatives, accounting for approximately 8% of the total GWP. It is worth noting that the proportions of construction GWPs for a simple overlay (treatment A) and CIR (treatment D) are even lower than that of transportation stage, representing only 2.1% and 3.2% of the total life-cycle GWP, respectively.

Figure 10(b) presents the breakdown of GWP by upstream and downstream fuel consumption, specifically fuel production and fuel use. The illustration clearly demonstrates that a 50-50 split rule is observed for the GWPs of all treatments (A, B, C, and D). This signified the equally important roles of the environmental-friendly techniques played in fuel production for energy supply and fuel combustion for user end. Fluctuations in either component can vitally affect the overall GWP of pavement

during its life cycle.

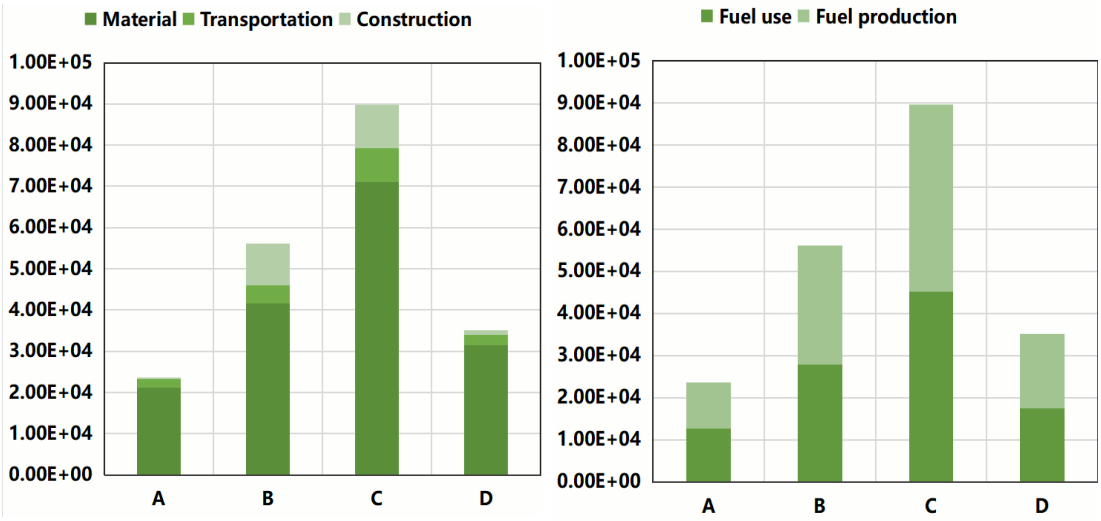

(a) (b)

Figure 10. GWP result breakdowns: (a) Life cycle stage breakdown; (b) Fuel consumption breakdown.

4.3 Cost performance

Figure 11 presents the LCCA results for treatment A, B, C, and D. Among the four alternatives, treatment A had the lowest expense per functional unit, while treatment C had the highest cost. Additionally, when compared to treatment C, which can also repair the upper and middle layers, CIR (treatment D) had an overall cost that was 45.8% lower.

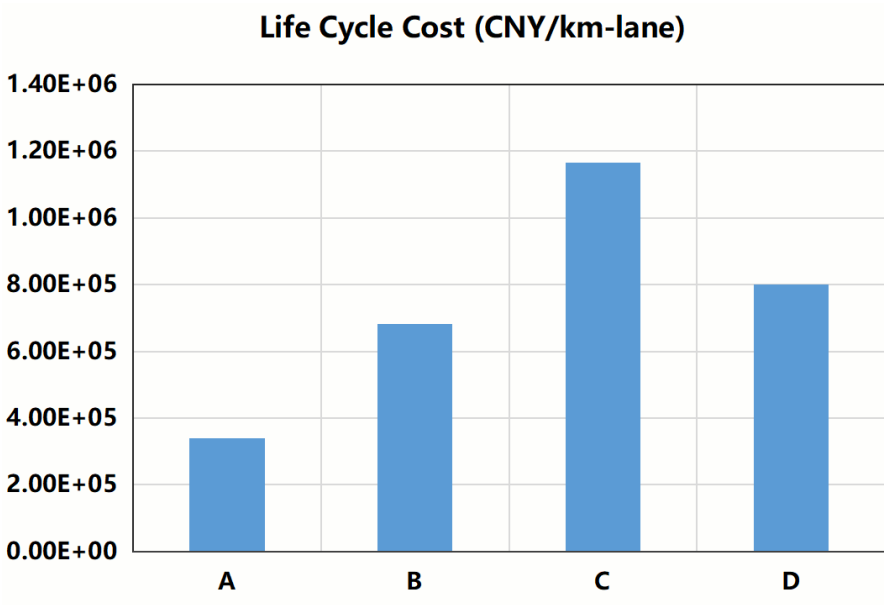

Figure 11. Life cycle cost results of treatment A, B, C, and D

The life cycle costs for the four M&R alternatives were analyzed based on breakdowns of cost types and construction activities (see Figure 12).

Figure 12(a) illustrates the distribution of costs among different components for treatment A, B, C, and D. The costs were categorized into labor, material, and construction machinery. Overall, it is evident that material expenses accounted for the highest proportion, ranging from 69.5% to 83.7%, exceeding half of the overall costs. Notably, the material cost for CIR (treatment D) constituted the highest proportion (83.6%) of its total cost, ranking second among all alternatives, although it involved recycling technology. As the material cost refers to the expenses beyond the sum of original price of the materials, which also includes the cost associated transportation, expenses related to the loss of materials during transportation, procurement fees,

storage fee, on-site storage fees, and storage losses. On the other hand, labor costs as a proportion of total costs are much lower (0.21% - 2.11%), with treatment D (CIR) having the lowest labor cost among all treatments. Moving on to construction machinery cost, this refers to expenses incurred for the use of rental construction machinery during construction operations, including depreciation expenses, major repair expenses, regular maintenance expenses, installation and removal expenses as well as fuel and power expenses. The proportional structure of construction machinery costs in treatment A, B, and C is similar, with a slight increase (26.1% - 28.3%), while the construction machinery cost for treatment D (CIR) only accounts for 16.11% of its total cost.

Figure 12(b) exhibits the cost breakdown for treatments A, B, C, and D based on different construction activities, including milling of the old surface layer, construction of new surface layers in different materials (SMA-13, AC-13, SUP-20), as well as CIR operation. For treatment B and C, it is evident that the cost of milling activity accounts for a small proportion of the total cost, approximately 4.2%-6.2%. It can also be observed that when the construction thickness is the same (4cm), the evaluated cost of SMA-13 is 7.9% higher than that of AC-13. However, when the construction thickness varies, the cost of constructing SUP-20 (6cm) is 40.8% and 30.5% higher than that of SMA-13 and AC-13, respectively, with 2cm additional layer thickness, despite SUP-20 having the lowest unit construction and installation cost among the three. The cost of

CIR operation is similar to the cost of constructing a 4cm layer using SMA-13 and AC-13. Nevertheless, the CIR operation can involve both the layer and middle layer with reaching up to 10cm treatment thickness, allowing for greater cost efficiency.

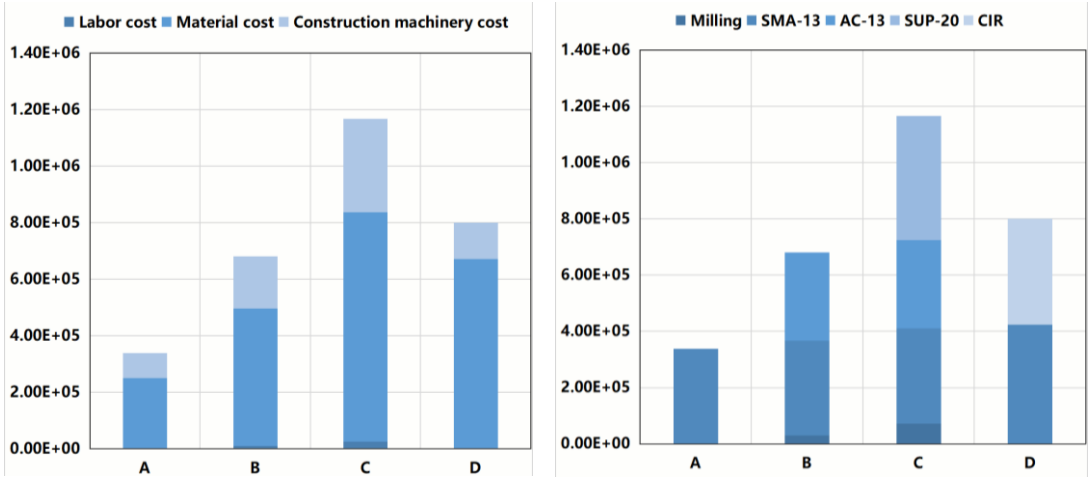

(a) (b)

Figure 12. LCCA result breakdowns: (a) Cost type breakdown; (b) Construction activity breakdown.

4.4 Nexus analysis

Figure 13 illustrates the relative environmental, economic, and technical performance of the four treatment alternatives for two different levels of pre-treatment pavement conditions. The x-axis represents the environmental impact, measured by the relative value of GWP, where a smaller value indicates lower environmental impact compared to the average level. The y-axis represents economic performance, indicating the relative cost performance, with a lower value indicating lower cost compared to the average level. The size of the bubbles reflects the improvement in rutting resistance

performance (creep rate) produced by different treatments relative to the corresponding pre-treatment performance.

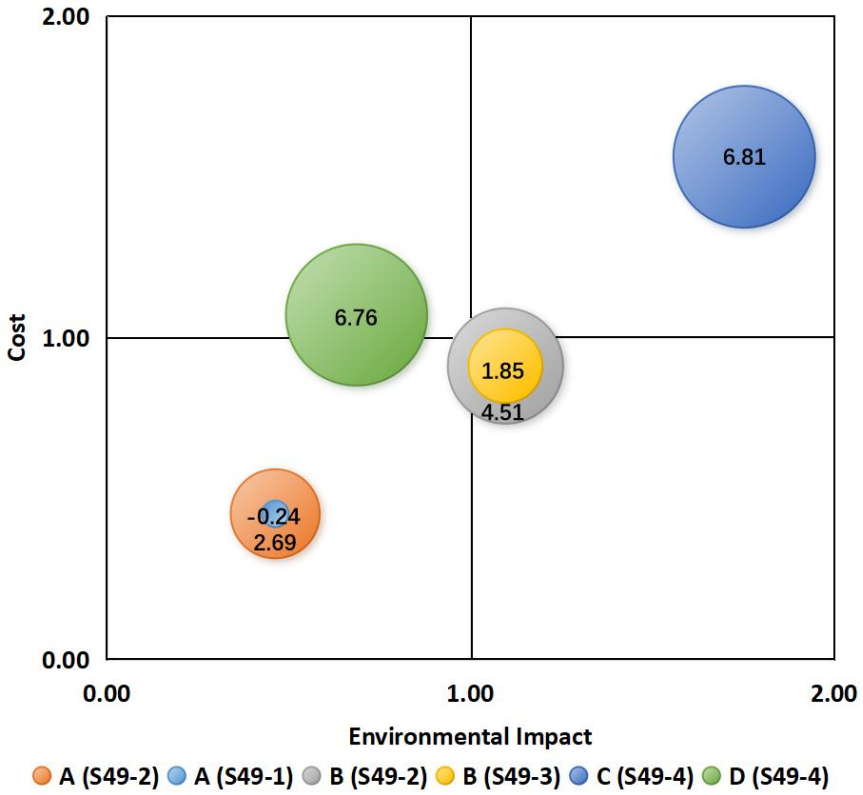

Figure 13. Modified Boston Matrix for nexus analysis

Nexus analysis was conducted based on the results shown in Figure 13 to assess the synergies and trade-offs among the four treatments. In terms of synergies, the environmental impacts and costs of treatment A (single overlay), B (M&F upper layer then overlay), and C (M&F upper and middle layers the overlay) showed an increasing trend as the number of treated pavement layers increases. Correspondingly, the improvement in rutting resistance performance also significantly enhanced with the increased bubble size (A to C). Treatment C performed the best in terms of rutting

resistance improvement, regardless of the pre-treatment pavement condition. It is worth noting from Table 6 that the pre-treatment rutting resistance of S49-2 pavement section is much worse than that of S49-1 and S49-3 sections. Combining this with the relative sizes of bubbles A (S49-1), A (S49-2), B (S49-2), and B (S49-3), it can be seen that the poorer the pre-treatment condition, the greater the improvement in rutting resistance after applying the same treatment. In terms of trade-offs, treatment B performed at an average level in environmental, economic, and technical aspects. However, it is worth mentioning that CIR treatment (D) achieved a better trade-off among environmental impact, cost, and rutting resistance improvement with slightly higher cost compared to treatment B. Specifically, among the four treatments compared, CIR (treatment D) can achieve the maximum improvement in technical performance similar to that of treatment C, while maintaining lower environmental impact and cost compared to the average levels.

5 Conclusions

This study quantified and compared the CIR treatment with three conventional M&R treatments in terms of maintenance effectiveness, environmental impacts, and cost perspectives. This was achieved through MSRL test, LCA, and LCCA methods. The quantification results were then integrated using a modified BGC Matrix in a nexus analysis to consider all dimensions. Results from this study have led to the following findings:

- The CIR technique shows remarkable performance recovery in compressive loading resistance, especially for full-depth pavement structures, it can achieve the comparable technical performance to the conventional maintenance treatment, while reducing GHG emissions by 60.8% and cost by 45.8%.
- The initial state of the pavement structure is a critical factor in determining the outcomes of maintenance interventions. It affects the effectiveness of repairs, the selection of appropriate interventions, and the overall cost-effectiveness of maintenance strategies.
- For all maintenance treatments in this study, the material-related impacts, whether in terms of GWP (74.14%-89.75%) or cost (69.5%-83.6%), accounted for the largest proportion in the overall amount.
- The nexus analysis provides a framework to assess the interdependencies between various factors and identify potential synergies, enabling more sustainable and cost-effective decision-making in pavement treatment and maintenance.

Although GWP was chosen as the representative indicator to specifically address the climate change impact of the evaluated activities, it is crucial to recognize that GWP is not the sole metric for evaluating environmental performance. Other indicators, such as energy consumption, resource depletion, and land use, could be taken into account in future studies to provide a more holistic assessment of the environmental performance.

In addition, while the creep test provides valuable information about rutting performance, it's crucial to consider fatigue resistance as well, especially at medium and low temperatures. Future studies are suggested to focus on evaluating and predicting the material's behavior under fatigue loading to gain a comprehensive understanding of the material's performance under different conditions.

In general, this study has established a nexus analysis framework to systematically compare the performance of pavement M&R treatment from various aspects, thus interconnecting multi-dimensional indicators. The compared results of CIR technique with other M&R treatments have filled a gap in previous research and provide valuable reference for decision-makers and future research endeavors. The implementation of this framework demonstrates its potentials in supporting integrated planning and management, as well as identifying ways to further improve sustainability.

6 Reference

Babashamsi, P., Md Yusoff, N. I., Ceylan, H., Md Nor, N. G., & Salarzadeh Jenatabadi, H. (2016). Evaluation of pavement life cycle cost analysis: Review and analysis. *International Journal of Pavement Research and Technology, 9*(4), 241-254. doi:10.1016/j.ijprt.2016.08.004

Babashamsi, P., Yusoff, N. I. M., Ceylan, H., Nor, N. G. M., & Jenatabadi, H. S. (2016). Evaluation of pavement life cycle cost analysis: Review and analysis. *International Journal of Pavement Research and Technology, 9*, 241-254.

Barksdale, H. C., & Harris, C. E. (1982). Portfolio Analysis and the Product Life Cycle. *Long Range Planning, 15*(6), 74-83.

Cao, R., Leng, Z., & Hsu, S.-C. (2019). Comparative eco-efficiency analysis on asphalt pavement rehabilitation alternatives: Hot in-place recycling and milling-and-filling. *Journal of Cleaner Production, 210*, 1385-1395.

doi:10.1016/j.jclepro.2018.11.122
Cao, R., Leng, Z., Yu, H., & Hsu, S.-C. (2019). Comparative life cycle assessment of warm mix technologies in asphalt rubber pavements with uncertainty analysis. *Resources, Conservation and Recycling, 147*, 137-144. doi:10.1016/j.resconrec.2019.04.031
Chappat, M., & Bilal, J. (2003). *The Environmental Road of the Future : Life Cycle Analysis : Energy Consumption & Greenhouse Gas Emissions*. Retrieved from
Chehovits, J., & Galehouse, L. (2010). *Energy usage and greenhouse gas emissions of pavement preservation processes for asphalt concrete pavements*. Paper presented at the First International Conference on Pavement Preservation, Newport Beach, CA.
Chinese Academy of Environmental Planning, Beijing Normal University, Sun Yat-Sen University, & Group, C. C. G. G. W. (2022). *China Products Carbon Footprint Factors Database(2022)*. Retrieved from Beijing, China:
Chiu, C.-T., Hsu, T.-H., & Yang, W.-F. (2008). Life cycle assessment on using recycled materials for rehabilitating asphalt pavements. *Resources, Conservation and Recycling, 52*(3), 545-556. doi:10.1016/j.resconrec.2007.07.001
De Pascale, B., Tataranni, P., Lantieri, C., Bonoli, A., & Sangiorgi, C. (2023). Innovative 100% RAP cold in-situ recycling of wearing course layers: laboratory and field characterisation and environmental impact assessment. *International Journal of Pavement Engineering, 24*(1). doi:10.1080/10298436.2023.2241099
EPA, U. (2021). *Exhaust and Crankcase Emission Factors for Nonroad Compression-Ignition Engines in MOVES 3.0.2*. Retrieved from United States Environmental Protection Agency:
Eurobitume. (2011). *Life Cycle Inventory: Bitumen*. Retrieved from European Bitumen Association:
Gao, L., Li, H., Xie, J., & Yang, X. (2017). Mixed-mode fracture modeling of cold recycled mixture using discrete element method. *Construction and Building Materials, 151*, 625-635.
Gao, L., Ni, F., Ling, C., & Yan, J. (2016). Evaluation of fatigue behavior in cold recycled mixture using digital image correlation method. *Construction and Building Materials, 102*, 393-402.
Giani, M. I., Dotelli, G., Brandini, N., & Zampori, L. (2015). Comparative life cycle assessment of asphalt pavements using reclaimed asphalt, warm mix technology and cold in-place recycling. *Resources, Conservation and Recycling, 104*, 224-238. doi:10.1016/j.resconrec.2015.08.006
Giustozzi, F., Toraldo, E., & Crispino, M. (2012). Recycled airport pavements for achieving environmental sustainability: An Italian case study. *Resources, Conservation and Recycling, 68*, 67-75. doi:10.1016/j.resconrec.2012.08.013
Grünig, R., & Kühn, R. (2018). *The Strategy Planning Process: Analyses, Options,*

Projects (Second Edition ed.): Springer.

Gu, F., Ma, W., West, R. C., Taylor, A. J., & Zhang, Y. (2019). Structural performance and sustainability assessment of cold central-plant and in-place recycled asphalt pavements: A case study. *Journal of Cleaner Production, 208*, 1513-1523.

Gu, X., Dong, Q., & Yuan, Q. (2014). Development of an innovative uniaxial compression test to evaluate permanent deformation of asphalt mixtures. *Journal of Materials in Civil Engineering, 27*(1), 04014104.

Ha, J., Yu, C., & Hwang, Y. (2021). Analyzing the impact of relative push and pull factors on inbound medical tourism in South Korea: focused on BCG matrix applied segment group characteristics. *Asia Pacific Journal of Tourism Research, 26*(7), 768-779. doi:10.1080/10941665.2021.1908387

INDOT. (2005). *Life Cycle Cost Analysis for INDOT Pavement Design Procedures*. Retrieved from INDOT:

IPCC. (2006). *2006 IPCC guidelines for national greenhouse gas inventories*. Retrieved from Intergovernmental Panel on Climate Change:

IPCC. (2021). *Climate Change 2021: The Physical Science Basis*. Retrieved from

IPCC. (2023). *Climate Change 2023: Synthesis Report. Contribution of Working Groups I, II and III to the Sixth Assessment Report of the Intergovernmental Panel on Climate Change*. Retrieved from Geneva, Switzerland:

ISO. (2006). Environmental management — Life cycle assessment — Principles and framework. In (Vol. ISO 14040:2006(E)). Switzerland: IHS.

Jiang, J., Ni, F., Gao, L., & Lou, S. (2016). Developing an optional multiple repeated load test to evaluate permanent deformation of asphalt mixtures based on axle load spectrum. *Construction and Building Materials, 122*, 254-263.

Jiang, J., Ni, F., Zheng, J., Han, Y., & Zhao, X. (2018). Improving the high-temperature performance of cold recycled mixtures by polymer-modified asphalt emulsion. *International Journal of Pavement Engineering*, 1-8.

Khairat, G. M., & Alromeedy, B. S. (2016). Applying the BCG Matrix to Analyze Egypt's Tourism Competitiveness Position. *Minia Journal of Tourism and Hospitality Research, 1*(2), 1-21.

Kim, Y., Im, S., & Lee, H. D. (2010). Impacts of curing time and moisture content on engineering properties of cold in-place recycling mixtures using foamed or emulsified asphalt. *Journal of Materials in Civil Engineering, 23*(5), 542-553.

Liu, J., Hull, V., Godfray, H. C. J., Tilman, D., Gleick, P., Hoff, H., . . . Li, S. (2018). Nexus approaches to global sustainable development. *Nature Sustainability, 1*(9), 466-476. doi:10.1038/s41893-018-0135-8

Lu, D., Jiang, X., Tan, Z., Yin, B., Leng, Z., & Zhong, J. (2023). Enhancing sustainability in pavement Engineering: A-state-of-the-art review of cement asphalt emulsion mixtures. *Cleaner Materials, 9*. doi:10.1016/j.clema.2023.100204

Ma, Y., Zhou, H., Jiang, X., Polaczyk, P., Xiao, R., Zhang, M., & Huang, B. (2021).

The utilization of waste plastics in asphalt pavements: A review. *Cleaner Materials, 2*. doi:10.1016/j.clema.2021.100031

Masnadi, M. S., El-Houjeiri, H. M., Schunack, D., Li, Y., Roberts, S. O., Przesmitzki, S., . . . Wang, M. (2018). Well-to-refinery emissions and net-energy analysis of China's crude-oil supply. *Nature Energy, 3*(3), 220-226. doi:10.1038/s41560-018-0090-7

National Burea of Statistics. (2020). *China Energy Statistical Yearbook*. China Statistics Press: China Statistics Press.

Reigle, J. A., & Zaniewski, J. P. (2002). Risk-Based Life-Cycle Cost Analysis for Project-Level Pavement Management. *Transportation Research Record, 1816*.

Santos, J., Bryce, J., Flintsch, G., Ferreira, A., & Diefenderfer, B. (2014). A life cycle assessment of in-place recycling and conventional pavement construction and maintenance practices. *Structure and Infrastructure Engineering, 11*(9), 1199-1217.

Santos, J., & Ferreira, A. (2013). Life-cycle cost analysis system for pavement management at project level. *International Journal of Pavement Engineering, 14*(1), 71-84. doi:10.1080/10298436.2011.618535

Shen, L., Du, X., Cheng, G., Shi, F., & Wang, Y. (2021). Temporal-spatial evolution analysis on low carbon city performance in the context of China. *Environmental Impact Assessment Review, 90*. doi:10.1016/j.eiar.2021.106626

Singh, J. P. (2004). Development trends in the sensor technology: a new BCG matrix analysis as a potential tool of technology selection for a sensor suite. *IEEE Sensors Journal, 4*(5), 664-669. doi:10.1109/jsen.2004.833494

Siverio Lima, M. S., Hajibabaei, M., Hesarkazzazi, S., Sitzenfrei, R., Buttgereit, A., Queiroz, C., . . . Gschösser, F. (2021). Determining the Environmental Potentials of Urban Pavements by Applying the Cradle-to-Cradle LCA Approach for a Road Network of a Midscale German City. *Sustainability, 13*(22). doi:10.3390/su132212487

Stripple, H. (2001). *Life Cycle Assessment of Road - A Pilot Study for Inventory Analysis*. Retrieved from Swedish National Road Administration:

Thenoux, G., González, Á., & Dowling, R. (2007). Energy consumption comparison for different asphalt pavements rehabilitation techniques used in Chile. *Resources, Conservation and Recycling, 49*(4), 325-339. doi:10.1016/j.resconrec.2006.02.005

Turk, J., Mauko Pranjić, A., Mladenovič, A., Cotič, Z., & Jurjavčič, P. (2016). Environmental comparison of two alternative road pavement rehabilitation techniques: cold-in-place-recycling versus traditional reconstruction. *Journal of Cleaner Production, 121*, 45-55. doi:10.1016/j.jclepro.2016.02.040

Kyoto Protocol to the United Nations Framework Convention on Climate Change, (1998).

Paris Agreement, (2015).

US EPA. (2006). *Glossary of terms from the Life Cycle Assessment: Principles and*

Practices report (EPA/600/R-06/060). Retrieved from United States Environmental Protection Agency:

Wang, T., Xiao, F., Zhu, X., Huang, B., Wang, J., & Amirkhanian, S. (2018). Energy consumption and environmental impact of rubberized asphalt pavement. *Journal of Cleaner Production, 180*, 139-158. doi:10.1016/j.jclepro.2018.01.086

Wang, X., Gu, X., Dong, Q., Wu, J., & Jiang, J. (2018). Evaluation of permanent deformation of multilayer porous asphalt courses using an advanced multiply-repeated load test. *Construction and Building Materials, 160*, 19-29.

Xiao, F., Yao, S., Wang, J., Li, X., & Amirkhanian, S. (2018). A literature review on cold recycling technology of asphalt pavement. *Construction and Building Materials, 180*, 579-604.

Yao, L., Dong, Q., Jiang, J., & Ni, F. (2019). Establishment of Prediction Models of Asphalt Pavement Performance based on a Novel Data Calibration Method and Neural Network. *Transportation Research Record, 2673*(1), 66-82.

Zarrinkamar, B. T., & Modarres, A. (2020). Optimizing the asphalt pavement cold in-place recycling process containing waste pozzolans based on economic-environmental-technical criteria. *Journal of Cleaner Production, 242*.

Zhou, F., & Scullion, T. (2002). Discussion: Three stages of permanent deformation curve and rutting model. *International Journal of Pavement Engineering, 3*(4), 251-260.